ACS Chemical Neuroscience pubs.acs.org/acschemicalneuroscience Article

Photochemically Initiated Intracellular Astrocytic Calcium Waves in Living Mice Using Two-Photon Uncaging of IP_3

Sarah E. Crowe,† Srinivas Kantevari,† and Graham C. R. Ellis-Davies*

Department of Neuroscience, Mt. Sinai School of Medicine, One Gustave Levy Place, New York, New York 10029, and Department of Pharmacology & Physiology, Drexel University College of Medicine, 245 North 15th Street, Philadelphia, Pennsylvania 19102

Abstract

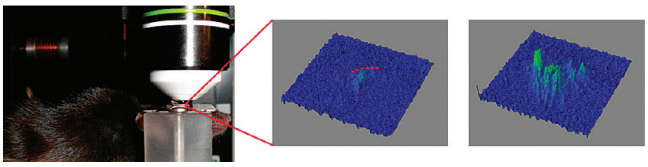

We have developed a caged IP_3 analogue for two-photon photolysis in living animals. This probe is a cell permeable version and was coloaded with a fluorescent Ca^{2+} dye into astrocytes in layer 1 of the somatosensory cortex of anesthetized mice. Two-photon irradiation of single cells at 720 nm produced rapid and robust increases in intracellular Ca^{2+} concentrations monitored using two-photon microscopy at 950 nm. The photoevoked intracellular Ca^{2+} waves were similar in magnitude to intrinsic signals in wild type mice. These waves did not propagate to other cells beyond the targeted astrocyte. In contrast, we observed intercellular astrocytic Ca^{2+} waves in two mouse models of familial Alzheimer's disease. These data suggest that Alzheimer's might perturb gliotransmission but not IP_3 signaling per se in mouse models of the disease.

Fluctuations in the concentrations of ionized intracellular calcium $[Ca^{2+}]_i$ are one of the most important and ubiquitous signaling processes in living cells (*1*, *2*). For example, $[Ca^{2+}]_i$ regulates the movement of many cells types, including all three types of muscle fibers, locomotion of white blood cells, neuronal growth cones, etc. $[Ca^{2+}]_i$ also regulates excitation−secretion coupling of intracellular vesicles with the plasma membrane in many cell types and thus the release of a diverse array of neuroactive substances (Glu, dopamine, serotonin, glycine, GABA, ATP, many small peptides, trophic factors, etc.) from cells in the central nervous system (CNS). Changes in $[Ca^{2+}]_i$ also initiate the secretion of hormones from neuroendocrine cells through the body (e.g., insulin release from the pancreas). Many fundamental processes in the birth, division, and death of organisms and cells are also controlled by $[Ca^{2+}]_i$. Since fluctuations in $[Ca^{2+}]_i$ are so central to the life of organisms, it is no surprise that the ability to monitor and manipulate $[Ca^{2+}]_i$ has been a major focus of organic chemists for more than 30 years. The development of fluorescent indicators to monitor $[Ca^{2+}]_i$ by Roger Tsien and co-workers in the 1980s has proved to be the seminal contribution to our understanding of intracellular Ca^{2+} signaling (*3*, *4*). The development of caged $[Ca^{2+}]_i$ probes went virtually hand-in-hand with these $[Ca^{2+}]_i$ dyes. Thus, there have been hundreds of studies of Ca^{2+} signaling in the CNS combining both probe types to provide a quantitative description of the effects of fluctuations in $[Ca^{2+}]_i$ (*5*).

Neurons in the CNS use both electrical and chemical signaling for communication. For example, glutamatergic synapses convert the presynaptic action potential into Ca^{2+}-driven transmitter secretion, which is in turn converted into a postsynaptic membrane current. Apart from the principal cells of the CNS, there are many other cell types that play vital supporting roles, either supplying neurons with essential nutrients or protecting them from damage. Glia are, in fact, the most numerous cell type in the CNS, outnumbering neurons by a factor of 10. One type of glia, astrocytes, are so entwined with neurons, that it is estimated that each astrocyte makes contact with more than 100,000 neuronal synapses (*6*). So intimate is this association of astrocytes and neuronal synapse that their juxtaposition has been dubbed a tripartite synapse. In the past 15 years, it has become clear that through this tripartite synapse, astrocytes not only provide vital support functions for neurons but also actively modulate their signaling (*7*−*9*).

Since astrocytes are not electrically excitable, fluctuations in $[Ca^{2+}]_i$ are the "language by which these cells talk" (*7*). Simply put, as action potentials are to neurons, so changes in $[Ca^{2+}]_i$ are to astrocytes. The main route for this mobilization of $[Ca^{2+}]_i$ is through phospholipase C (PLC) release of inositol-1,4,5-trisphosphate (IP_3) from the lipid PIP_2. This IP_3 increases the open channel probability of a Ca^{2+} channel on the endoplasmic reticulum, allowing intraorganelle calcium to escape from this store to cause an increase in cytosolic calcium ($[Ca^{2+}]_i$). The signaling cascade is terminated by IP_3 5-phosphatase hydrolyzing IP_3 to IP_2 and Ca^{2+} pumps

Received Date: May 26, 2010
Accepted Date: May 28, 2010
Published on Web Date: June 15, 2010

DOI: 10.1021/cn100052v | *ACS Chem. Neurosci.* (2010), *1*, 575–585

reducing $[Ca^{2+}]_i$ to resting values. This is the canonical Ca^{2+} signaling mechanism in astrocytes (*7*, *8*). It is no surprise therefore that several diseases are reported to be associated with perturbations in astrocytic Ca^{2+} (*9*); however, the exact role of such $[Ca^{2+}]_i$ signaling on astrocytic modulation of neuronal function remains controversial (*8*). Optical methods that allow neuroscientists to control astrocytic $[Ca^{2+}]_i$ with single cell or even subcellular precision are a highly desirable goal. Photolytic uncaging of a very wide variety of signaling molecules has been used to study many types of cultured cells (*10*, *11*). In the current work, we report in detail the efficient synthesis of a cell permeant caged IP_3 that undergoes effective two-photon uncaging in intact astrocytic cells in the cortex of living mice. The photolytically evoked intracellular Ca^{2+} transients were compared to intrinsic (or spontaneous) Ca^{2+} signals in healthy mice and those having transgenes from humans having mutations that give rise to familial Alzheimer's disease (FAD (*12*)). We found that two-photon uncaging of IP_3 *in situ* could mimic the former but not the latter, suggesting FAD mutants disrupt astrocytic Ca^{2+} without perturbing IP_3-signaling per se.

Results and Discussion

Synthesis

The synthesis of the caged IP_3 analogue (**1**) used for these studies is outlined in Scheme 1. Starting with the known (±)-2,3−4,5-di-*O*-cyclohexilydene-6-*O*-(*ortho*-nitroveratryl)-*myo*-inositol (**2**)(*13*), the 1-hydroxyl functionality was derivitized with (1*S*)-(−)-camphanic chloride to give **3** in 85% yield. The cyclohexilydene protecting group on the 4,5-dihydroxy functionality was then selectively removed by treatment with acetyl chloride (3% solution for 20−25 min). It should be noted that higher concentrations of chloride or longer treatment times with lower concentrations concomitantly removed the second cyclohexilydene, greatly hindering the isolation of pure **4** in good yield. Other acids (e.g., TFA (*14*)) were also found to be much less selective for this key transformation. Crude **4** was sufficiently pure for the next, simple base hydrolysis of the camphanylic ester to triol **5** in a high yield for two steps. Triol **5** was phopsphitylated with freshly prepared *N*,*N*-diisopropyl-bis(2-cyanoethyl)-phosphoramidite (six equivalents were important for a good yield). The progression of the reaction was carefully monitored by TLC over a period of 16−24 h. TLC showed a succession of spots of higher R_f compared to that of **5** (mixtures of mono- and bisphosphitylates). After approximately one day at RT, TLC analysis of the reaction mixture showed essentially one product, the desired trisphosphitylated intermediate target. Once a single spot predominated, the RM was cooled with an ice−water bath to ca. 4 °C and treated with *tert*-BuOOH for 1 h to give trisphosphate **6**. The integrity of this synthetic sequence was verified by the conversion of **6** with Hunig's base then Dowex H^+ to give (±)-6-*O*-(*ortho*-nitroveratryl)-*myo*-inositol 1,4,5-trisphosphate (**7**) and comparison of ^1H and ^{31}P NMR spectra with those from material synthesized with different reagents (*13*). Thus satisfied with the structural integrity of **6**, we treated this intermediate with Hunig's base for 18 h, then acetoxymethylbromide (AM-Br) and Hunig's base in dry acetonitrile at RT for 19 h. The progress of the reaction was monitored with reverse-phase HPLC, which revealed a complex pattern of deprotection of cyanoethyl groups and reprotection of the phosphate with AM-Br. The reaction reached an apparent end point with one major product visible by HPLC and TLC. Several other more polar components were visible: mixtures of cyanoethyl- and AM-protected phosphates. The target caged compound (**1**) was isolated in 35% yield from **6**, implying ca. 84% for each deprotection/reprotection reaction.

The key step in synthetic Scheme 1 was the discovery that complete deprotection of the advanced synthetic intermediate **6** was not required for efficient construction of the hexakis-AM ester. Indeed, we found that hemi deprotection was the best route for protecting group exchange. This aspect of AM ester synthesis has not been reported in the literature before. The efficient synthesis of compound **1** has already allowed us to study the effects of astrocytic calcium signaling on glutamatergic synapses in magnocellular neurosecretory cells in the hypothalamic paraventricular nucleus by 2P uncaging in acute brain slices (*15*). Only two examples of UV uncaging of other molceules *in vivo* (i.e., in living animals) have been reported (*16*, *17*); in this work, we extend the 2P uncaging method to living mice for the first time.

When AM-ester derivatives of dyes and probes are applied at low concentrations to living cells, they pass through the plasma membrane; once inside the cells, the esters are hydrolyzed by intracellular esterases, thus trapping the free acid and allowing more probes to partition into the cytosol (*3*) (Scheme 1). Depending on the probe, quite high concentrations of dyes can be loaded into living cells using this method, thus allowing optical methods of sensing and actuation to be applied to the intracellular environment without disrupting either the plasma membrane or any intracellular constituents. For our imaging of $[Ca^{2+}]_i$ using the two-photon microscopy shown below, we loaded the fluorescent Ca^{2+} indicators fluo-4 or X-rhod-1 via their AM esters into astrocytes in the cortex of living mice (*18*). In the uncaging experiments, we coloaded **1** with the calcium dye, and the intracellular esterases removed the six AM ester protecting groups to reveal three phosphate moieties, converting **1** to **8** *in situ*. Photolysis of **8** inside cells gives the IP_3 cyclohexilydene analogue **9**, which can effectively mobilize intracellular Ca^{2+}, as

DOI: 10.1021/cn100052v | *ACS Chem. Neurosci.* (2010), *1*, 575–585

Scheme 1. Synthesis of the Cell Permeant Caged IP3 Analogue[a]

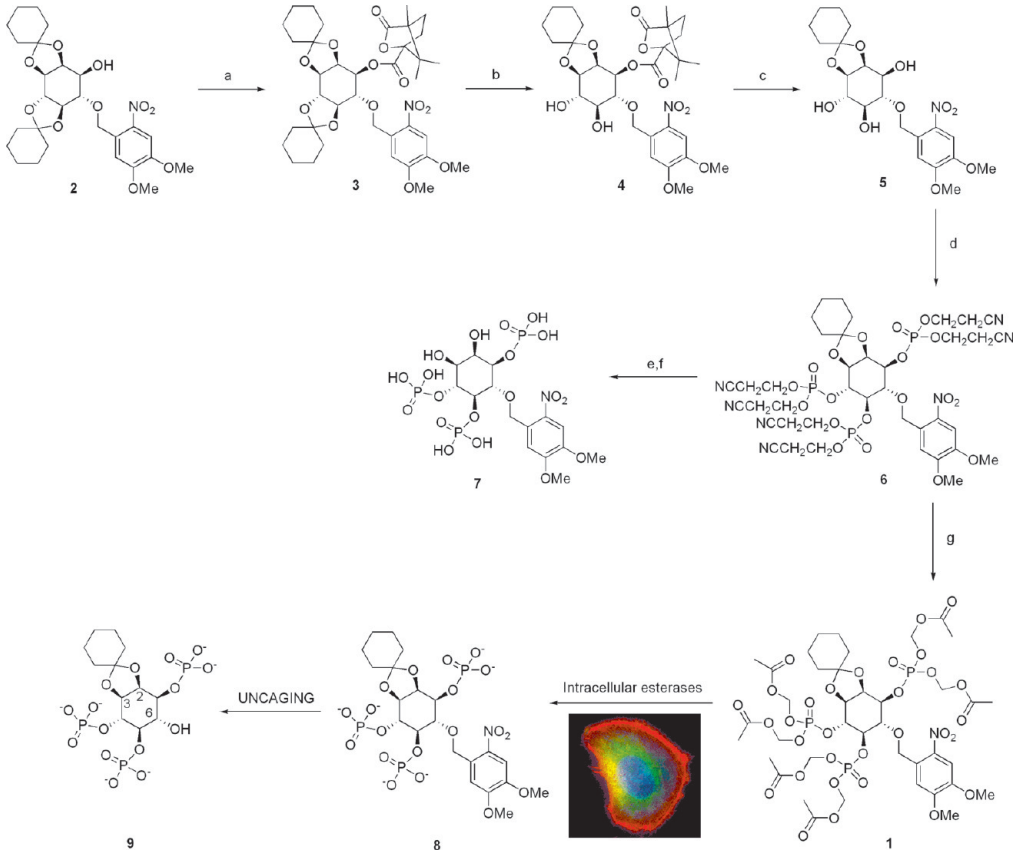

[a] Reagents and conditions: (a) camphanic chloride, TEA, RT, 18 h; (b) acetyl chloride, RT; (c) KOH, RT, 18 h; (d) $(^{i}Pr)_2NP(CH_2CH_2CN)_2$, tetrazole, RT, 18 h then ^{t}BuOOH 0 °C, 1 h; (e) Hunig's base; (f) Dowex-H^+; (g) AM-Br, Hunig's base, RT, 18 h. Inside cells, compound **1** reacts with intracellular esterases that hydrolyze the AM esters, thus liberating the phosphates. Uncaging cleaves the benzyl ether, releasing the 6-hydroxyl functionality.

only the 6-hydroxyl is essential for opening the IP_3-gated ER Ca^{2+} channel (*13*). The receptor is quite tolerant of IP_3 bearing substituents at the 2 and 3 hydroxyls and even the 1-phosphate.

Two-Photon Imaging of Astrocytes and Neurons in Living Mice

In the past decade, the two-photon microscope has enabled imaging of astrocytes and neurons in living mice (*19*). Both genetically encoded probes and chemically synthesized dyes have proved extremely effective for imaging single cells with exquisite detail in the neocortex of living rodents. The fine structure of astrocytes and the lateral spatial disposition of individual cells are shown in Figure 1a, which shows a fluorescent image of the somatosensory cortex at a depth of about 60 μm below the pia surface in a transgenic mouse labeled with enhanced green fluorescent protein (eGFP) driven by the astrocyte-specific promoter GFAP (glia fibrillary acidic protein). The cell bodies of the astrocytes appear as large, intensely stained blobs projecting several arms that develop into a very finely divided web that is so fine that it appears almost like a mist (*6*). One of these arms is different from the others, projecting to a nearby blood vessel or capillary, which is then ensheathed in endothelia. Depending on the orientation of the capillary to the imaged x/y plane, the endothelia appear as a circle surrounding a black hole or continuous set of parallel tracks (see Figure 1a). Using these specialized structures, astrocytes deliver nutrients from the blood to neurons, recycle neurotransmitters, and directly modulate neuronal function (*7*, *9*).

Individual astrocytes are not only highly ramified, as described above, but also form a connected collective (or syncytium) in which each astrocyte is joined to its immediate neighbors via gap junctions. Thus, after removing the dura through a small craniotomy, we applied the specific astrocytic marker, SR101, to the surface of the cortex of a living mouse. As previously reported by Helmchen and co-workers, we could easily image hundreds of micrometers into the brain of an anesthetized mouse (*20*) (Figure 1b shows sections a 3D volume reconstruction). Fluorescent Ca^{2+} dyes may be loaded in a similar manner to SR101, by topical application of the AM ester to the pia, or they can be pressure injected into the brain at defined points below the pia (*21*). The

DOI: 10.1021/cn100052v | *ACS Chem. Neurosci.* (2010), *1*, 575–585

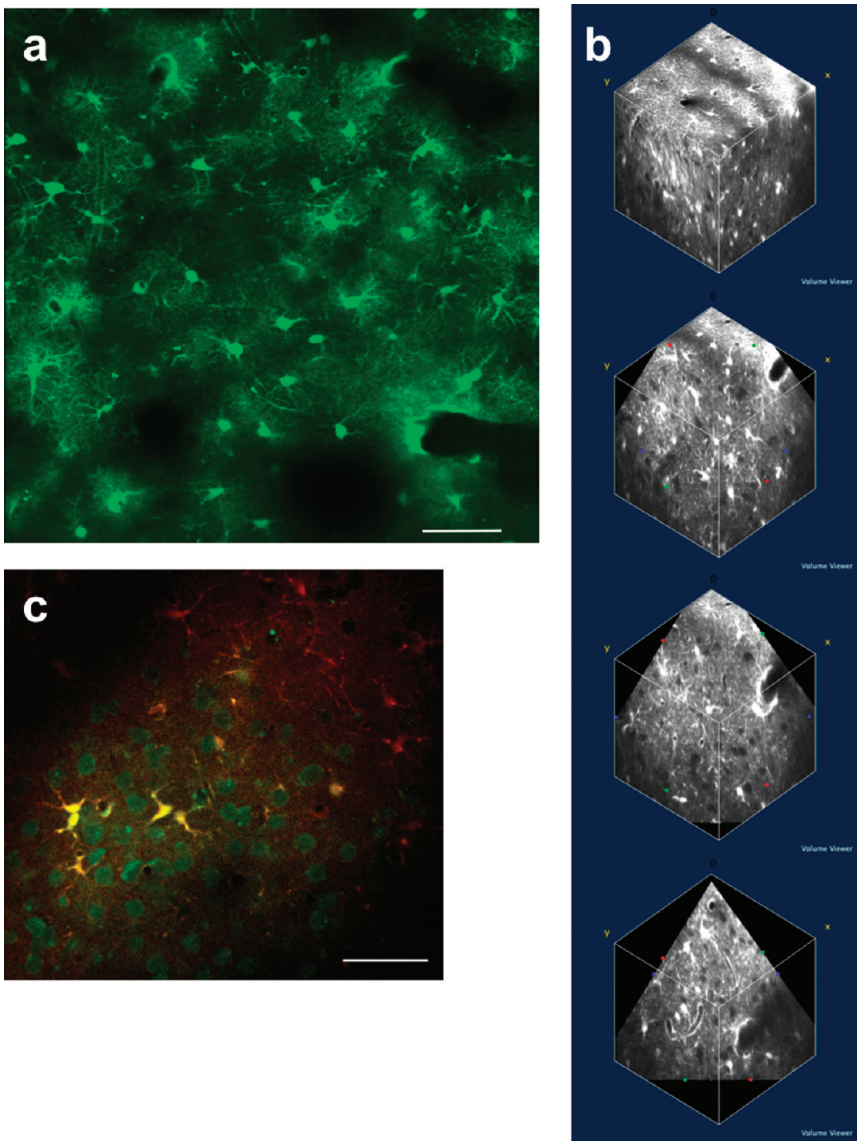

Figure 1. Two-photon imaging of astrocytes and neurons in living mice. (a) Fluorescent image of astrocytes from the neocortex of a living mouse. A single $x-y$ plane from a three-dimensional fluorescent image is shown in which each astrocyte is intensely labeled with eGFP driven by the astrocyte-specific GFAP promoter such that the fine cellular processes are clearly visible. (b) Four volume renderings of a 300-μm cube of the brain of a living mouse in which cells were acutely labeled with the astrocyte-selective fluorescent maker SR-101 by topical application to the pia. The volume shown was part of layers 1−3 of the neocortex. Single $x-y$ images were taken with a 2P microscope with a z-spacing of 2 μm. (c) Fluorescent image of astrocytes and neurons in layer 2/3 of a living mouse. Both cell types were labeled by bolus injection of the green Ca^{2+} dye fluo-4 as its AM ester in the brain via a patch pipet. Astrocytes were labeled with SR-101. Neurons only uptake fluo-4 and therefore are shown in green, but astrocytes uptake both dyes and therefore appear yellow or orange, depending upon the proximity to the injection site. The scale bar is 50 μm.

former method loads only astrocytes, whereas the latter loads astrocytes and neurons (Figure 1c). In Figure 1c, pyramidal neurons from layer 2 appear green (stained with the green Ca^{2+} dye fluo-4), and astrocytes appear either orange (SR101) or yellow (costained with SR101 and fluo-4) (*20*). For our studies of Ca^{2+} dynamics in astrocytes in living mice, we used topical loading of Ca^{2+} dyes (fluo-4 or X-rhod-1) as their AM esters (*18*), as pressure injection is time-consuming and loads only a very small fraction of cells near the injection point, whereas topical loading of probes is facile and selectively loads many hundreds of astrocytes.

Two-Photon Uncaging of IP_3 and Ca^{2+} Imaging in Astrocytes of Living Mice

A mixture of **1** and X-rhod-1/AM was applied to the surface of the pia of an anesthetized adult mouse (ca. 5 months age) as described in Methods. After 60 min, excess dyes were removed by irrigation with buffer, and the craniotomy was sealed with a glass coverslip, with

DOI: 10.1021/cn100052v | *ACS Chem. Neurosci.* (2010), *1*, 575–585

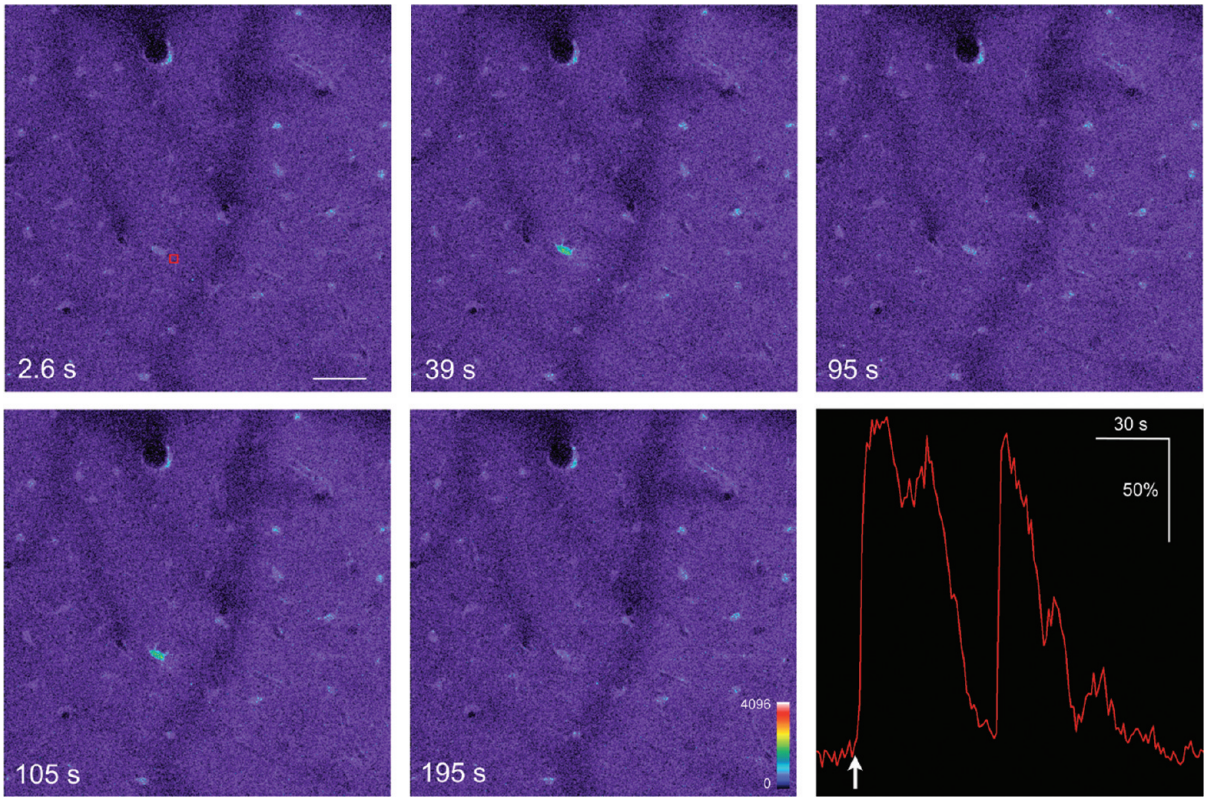

Figure 2. Two-photon uncaging of IP_3 *in vivo* evoked intracellular but not intercellular Ca^{2+} waves. Caged IP_3/AM (**1**) was coloaded into astrocytes with X-rhod-1 by topical application to the pia. Uncaging in an area encompassing the processes of one astrocyte (red box, frame 1) evoked an intracellular calcium wave that did not propagate to neighboring cells. Uncaging with a mode-locked Ti:sapphire laser was in a grid 4×4 points equally spaced within the box, with 15 mW at 720 nm for 20 ms per point. Imaging at 950 nm was at a frame rate of 1.3 s. Time stamp for the image frames shown is in seconds. The change in fluorescence due to the increase in $[Ca^{2+}]_i$ is shown on a 12-bit scale and is displayed graphically in the lower right panel (red trace). The arrow indicates the uncaging time point. Supporting Information movie 1 shows the change in fluorescence during the same period as $\Delta F/F$. The scale bar is 50 μm.

agarose filling the gap between the pia and glass. Two-photon imaging revealed that many astrocytes were stained with the Ca^{2+} dye (Figure 2). Our two-photon microscope has a frame rate of about 1 Hz for a single z-section, if we image x/y at high resolution (i.e., 512 pixels in each lateral dimension), and useful signal-to-noise (S/N) ratios (4 μs pixel dwell time). Since X-rhod-1 is an intensity-based dye, low magnification images such as those in Figure 2 are much grainier than those in Figure 1a. This is because at low $[Ca^{2+}]_i$ levels, the indicator is weakly fluorescent compared to eGFP; thus, only astrocyte cell bodies and some of their major processes and endothelia are apparent in Figure 2. At higher magnification and $[Ca^{2+}]_i$, much cellular detail is readily observed (Figure 3).

We used a Ti:sapphire Mira 900 laser mode-locked at 720 nm with a pulse-width of 100 fs and an energy of 25 mW at the objective back aperture for uncaging. Fifteen milliwatts leaves the objective lens with an unknown pulse-width (probably < 140 fs). At low magnification (frame size 360 μm), we tested two uncaging paradigms. First, uncaging in the cell body of an astrocyte at a single location for 20 ms produced robust and consistent increases in $[Ca^{2+}]_i$, as reported by increases in intensity of X-rhod-1 fluorescence monitored with a second Ti:sapphire laser mode-locked at 950 nm. Concerned that firing the uncaging laser directly at the cell body might cause changes in $[Ca^{2+}]_i$ itself, we developed a second uncaging paradigm at this low magnification. We selected a box adjacent to an astrocyte cell body (Figure 2) that must encompass many cell processes not visible at the chosen magnification and S/N ratio. Nevertheless, uncaging at 16 even spaced locations in this area produced $[Ca^{2+}]_i$ oscillations that were reproducible and nontoxic to the stimulated cell. We observed an initial $[Ca^{2+}]_i$ transient immediately after the first uncaging event, which was frequently followed by more $[Ca^{2+}]_i$ oscillations. This pattern of intracellular Ca^{2+} signaling could be reproduced in the same cell a number of times during a 20 min imaging session. Figure 2 shows a representative example of such repetitive signaling events. In the cells (85%, $n = 45$) that showed an increase in signal after IP_3 uncaging, 80% had at least one Ca^{2+} signal oscillation. Importantly, we never observed the evoked intracellular Ca^{2+} signal to propagate beyond the cell which we uncaged (Supporting

DOI: 10.1021/cn100052v | *ACS Chem. Neurosci.* (2010), *1*, 575–585

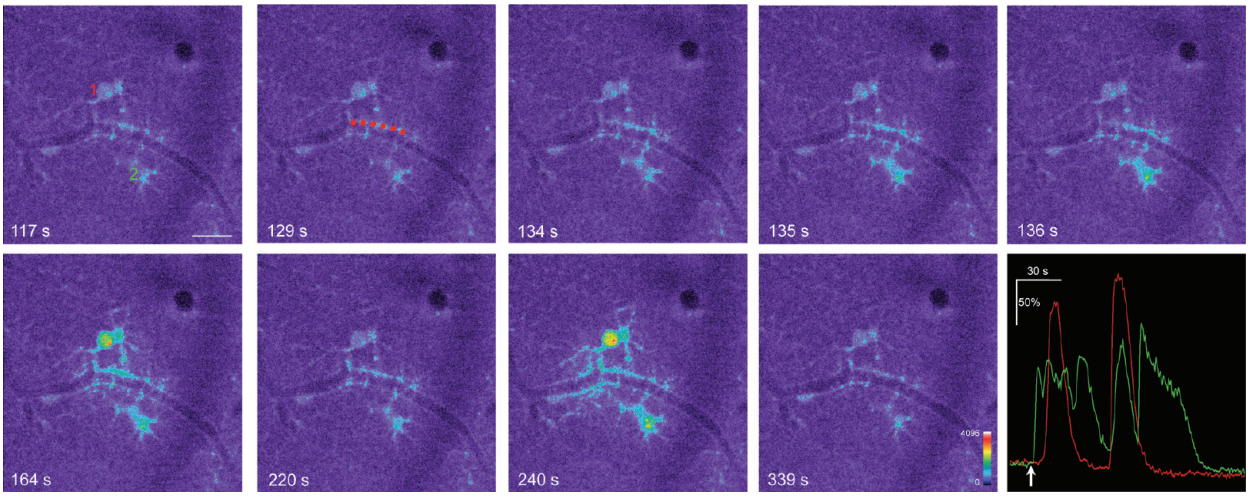

Figure 3. Local two-photon uncaging of IP_3 *in vivo* evoked oscillations in $[Ca^{2+}]_i$. Caged IP_3/AM (**1**) was coloaded into astrocytes with X-rhod-1 by topical application to the pia. Uncaging at six points (red dots, frame 2) evoked a rapid increase in $[Ca^{2+}]_i$ along the endothelia process that propagated as a wave to the two cells connected to this volume by their endfeet processes. Uncaging was at 133 s (immediately before frame 3), and thus, the rise in $[Ca^{2+}]_i$. appears instantaneous. The output from a mode-locked Ti:sapphire laser was 15 mW at 720 nm for 20 ms per point. Imaging at 950 nm was at a frame rate of 1.3 s. The time stamp for the image frames shown is in seconds. The change in fluorescence due to the increase in $[Ca^{2+}]_i$ is shown on a 12-bit scale and is displayed graphically in the lower right panel (red trace is from cell 1 and green from cell 2); the arrow indicates the uncaging time point. Supporting Information movie 2 shows the change in fluorescence during the same period. Scale bar 20 μm.

Information movie 1). In other words, *in vivo*, we could evoke no *intercellular* Ca^{2+} astrocytic waves, only *intracellular* Ca^{2+} waves by two-photon photolysis of caged IP_3.

We tested the threshold level for phototoxicity of these two uncaging paradigms by imaging $[Ca^{2+}]_i$ in animals in which only X-rhod-1 had been loaded. We found a significant difference between the energy levels required to evoke fluorescent responses with and without coloaded **1**. In the absence of **1**, we had to use 75 mW for 100 ms to evoke increases in fluorescence. In contrast to the photochemically evoked Ca^{2+} transients shown in Figure 2, when **1** was photolyzed at low energy, these higher energy increases in X-rhod-1 fluorescence never returned to baseline levels. Furthermore, at low power (i.e., 15 mW), we could evoke no phototoxic fluorescent signals even with ten times as many uncaging events used in Figure 2. The control experiments prove that the intracellular Ca^{2+} oscillations we observed at low power levels in the presence of **1** were due to intracellular two-photon uncaging of an IP_3 analogue. Interestingly, even at phototoxic energy levels, no intercellular Ca^{2+} waves were evoked.

Highly localized two-photon uncaging of **1** was also feasible. At 60× zoom, endothelial processes surrounding blood vessels are readily apparent. Figure 3 shows an example of two X-rhod-1-filled astrocytes connected to the same endothelium. Photolysis along one part of the process (Figure 3, red dots) produced rapid increases in dye fluorescence in both astrocytes, which could be seen to spread to much of their fine processes by diffusion (Figure 3 and Supporting Information movie 2). We believe that the simultaneous increase in signaling in both astrocytes is due to the entwining of the endfoot processes along the endothelium of the blood vessel, rather than cell-to-cell signaling. This would be consistent with the results seen at lower magnification. As with uncaging at low magnification, oscillations were seen that were evoked in a nontoxic and repetitive manner. We observed a rapid (<1 s) cellular response to optical stimulation that was within the time resolution of the full frame imaging rate of our 2P microscope.

Two-Photon Imaging of Intrinsic Astrocytic Ca^{2+} Signals in Normal Living Mice

Intrinsic changes in $[Ca^{2+}]_i$ inside astrocytes in layer 1 of the neocortex of living mice was monitored using 2P imaging. X-rhod-1 was loaded into wild type mice (age range: 5−7 months) as described in Methods. Under ketamine/xylazine anesthesia, we observed very few substantial changes (i.e., >20% above baseline fluorescence) in fluorescence in the cell bodies of dye-labeled astrocytes. Since each cell loads a different amount of dye, signals from monowavelength Ca^{2+} indicators such as X-rhod-1 and fluo-4 are always reported as change in fluorescence divided by the initial fluorescence for each cell (i.e., $\Delta F/F$). Thus, only relative, not quantitative, measurements of $[Ca^{2+}]_i$ are feasible. Even with the appropriate amount of anesthetic, there is always the chance that slight movement artifacts due to blood flow and respiration might contribute to such fluorescent imaging in living mice. In a normal field of view (360 × 360 μm), we imaged between 20 and 40

DOI: 10.1021/cn100052v | *ACS Chem. Neurosci.* (2010), *1*, 575–585

Table 1. Summary of the Intrinsic Astrocytic Calcium Signaling in Wild Type (WT) and PDAPP Mice[a]

	active astrocytes	total astrocytes	% active	signaling frequency (Hz)
WT ($n = 4$)	3	121	2.48 ± 0.3	0.00033 ± 0.00067
PDAPP ($n = 4$)	84	153	52.9 ± 2.41	0.0028 ± 0.0016
P-value			0.0056	0.046

[a] Twenty to 30 astrocytes were in the field of view (e.g., Figure 4b) during a typical 20 min imaging session. Cells that exhibited signals of 20% above the initial resting value were scored as active. Values are the mean ± SD.

astrocytes, typically for a 20 min period. We were careful to maintain the imaging laser with as low an energy as possible, while still being able to obtain decent S/N ratios. Thus, in all of the imaging sessions the energy at the back aperture of the 20× objective lens was always <20 mW and often <10 mW, depending on the quality of dye loading. During a standard imaging session, we observed approximately two spontaneous Ca^{2+} signals in the field of view (frequency $= 0.00033 \pm 0.00067$ Hz, $n = 121$ astrocytes from 4 mice; Table 1). The size and duration of the $\Delta F/F$ signal was similar to those evoked by the two-photon uncaging of IP_3.

Two-Photon Imaging of Intrinsic Astrocytic Ca^{2+} Signals in Transgenic Mouse Models of Alzheimer's Disease

We examined the effects of FAD mutants on astrocytic Ca^{2+} signaling in transgenic mouse models of AD with topically loaded X-rhod-1 and fluo-4. Urethane or ketamine/xylazine were used as anesthetics. The first mouse we examined was the 3xTgAD model (*22*). In one mouse, we observed very large spontaneous increases in fluorescence using fluo-4 under urethane anesthesia that propagated throughout the astrocyte network in the field of view at a rate of 2−3 μm per second (Figure 4a). We applied this observation and technique to the PDAPP mouse model (*23*). We saw that astrocytic Ca^{2+} signaling was perturbed in a similar way, with prominent intercellular Ca^{2+} waves that were not observed in wild type mice (Figure 4b, and Supporting Information movie 3). Furthermore, the frequency of large spontaneous intracellular astrocytic Ca^{2+} transients was significantly higher in PDAPP mice than wild type mice ($52.9 \pm 2.4\%$ of astrocytes signaled, $n = 153$ cells, frequency of signaling $= 0.0028 \pm 0.0016$ Hz, from 4 mice aged 14−16 months; Table 1).

Astrocytic Calcium Signaling and Alzheimer's Disease

Intercellular calcium waves have been observed in certain mouse models of disease states such as epilepsy (*24*, *25*), AD (*26*), and cortical spreading depression (*27*, *28*). Consistent with these reports, we observed astrocytic calcium waves in two mouse models of AD, the 3xTgAD (*22*), and the PDAPP (*23*). The 3xTgAD mouse overproduces human amyloid-beta (Aβ) because of the presence of three human transgenes (APP mutations: Lys670Asn and Met671Leu and presenilin1 mutation Met146Val). Mutant presenilin1 is also present in other mice reported to have hyperactive calcium signaling, and since this protein also affects calcium buffering (*29*) and signaling (*30*), it is not clear, *a priori*, whether plaques or dysregulated calcium stores cause hyperactivity (*31*). The PDAPP mouse model of AD has a single human APP transgene (APP Val717Phe) that shifts production of Aβ-40 to amyloidogenic Aβ-42 and is thus not confounded by presenilin1 mutations. Since PDAPP also shows hyperactivity astrocytic calcium signaling (Figure 4b), we suggest that presenilin1 mutations are not obligatory for the disruption of calcium signaling but that the over production of Aβ-42 and plaques per se is correlated with astrocytic calcium dysregulation. In the ages examined for both the 3xTg and PDAPP mice, Aβ plaques are found throughout the cortex. The 3xTg mouse line has plaque formation starting around 6 months. The PDAPP mouse line shows plaque formation around 9 months. Since uncaging of IP_3 did not generate hyperactive astrocytic calcium signaling or intercellular calcium waves, we would suggest that AD may perturb the release of ATP from astrocytes since this gliotransmitter has been shown to be involved in calcium waves *in situ* (*32*).

In 1990, the laboratory of Steve Smith reported "spontaneous" calcium waves in cultured astrocytic cells (*33*). This was the first suggestion that the astrocyte syncytium could participate in long-range signaling events in the CNS. At that time, this suggestion was very provocative since neurons were thought to be the only active signaling cells in the brain. It is now thought that such long-range intercellular calcium waves in astrocytes are probably an artifact of primary culture that grows cells in a monolayer on a glass coverslip (*8*). Thus, the connectivity and three-dimensional structure of astrocytes in culture are quite different from that seen in the brain of living animals (Figure 1). Recently, a handful of laboratories have reported the absence of intercellular calcium waves in astrocytes in normal living animals (*17*, *20*, *24*, *26*, *34*), and our results are consistent with such reports. We saw large calcium signals in the cell body of astrocytes at a very low frequency of ca. 0.1 Hz and in very few cells (ca. 2.5%). Two-photon uncaging of IP_3 allowed us to impose reproducibly large intracellular calcium transients at

DOI: 10.1021/cn100052v | ACS Chem. Neurosci. (2010), 1, 575–585

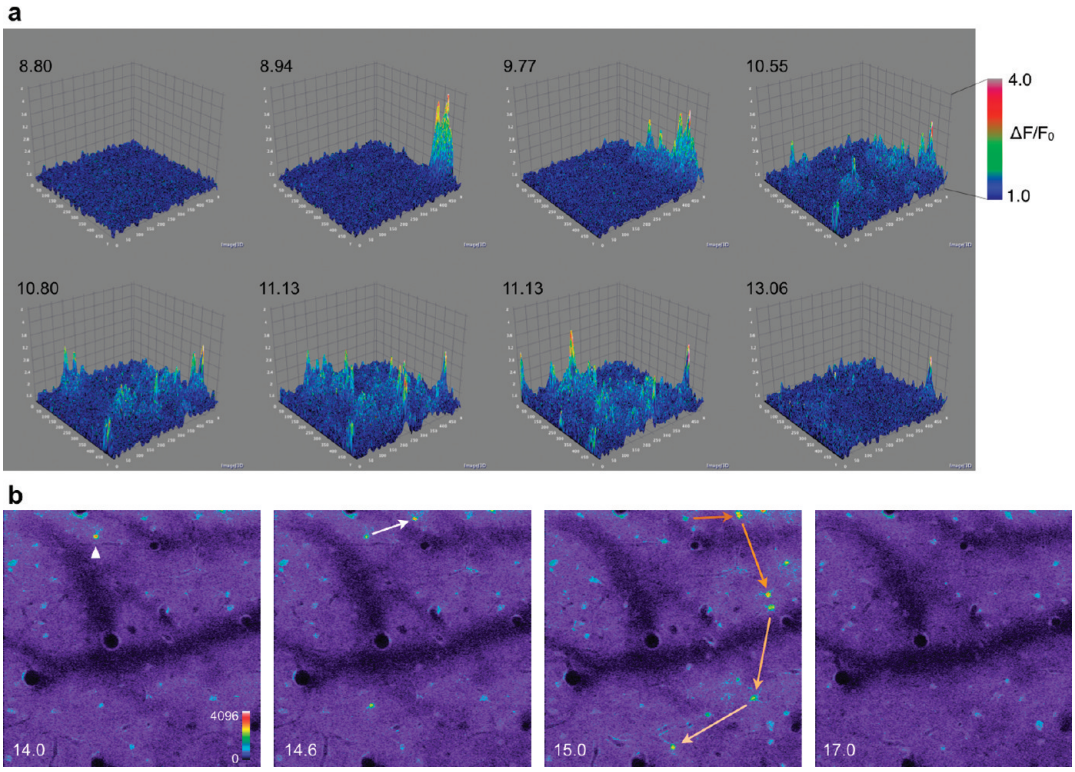

Figure 4. Two-photon imaging of intercellular astrocytic calcium waves in 3xTgAD and PDAPP mice. (a) The calcium-sensitive fluorescent indicator fluo-4 was selectively loaded into astrocytes of a female 3xTgAD mouse by topical application of its AM ester to the pia. Images of a single $x-y$ plane were taken every 3 s with a field of view of a 600 μm square. During the imaging session (20 min), the fluctuations in $[Ca^{2+}]_i$ were marked by both hyperactivity (many active astrocytes signaling frequently) and directional propagation. In the image frames shown, a major Ca^{2+} wave was seen to initiate in the lower right corner. No waves were observed in a background control mouse of 22 months. Changes in fluorescence ($\Delta F/F$) are shown on a pseudocolor scale that is also rendered as a surface plot. The time stamp is in mins. Supporting Information movie 3 shows the full 20-min imaging session where the change in fluorescence is on a 12-bit pseudocolor scale. (b) The calcium-sensitive fluorescent indicator X-rhod-1 was selectively loaded into astrocytes of a female PDAPP mouse by topical application of its AM ester to the pia. Images of a single $x-y$ plane were taken every 1.3 s with a field of view of a 360 μm square. An example of a calcium wave from a 16 month-old female mouse is shown, with the direction of propagation of a Ca^{2+} wave indicated by the arrows. Data from 4 mice are summarized in Table 1. The time stamp is in mins.

will, in visually selected cells in the astrocyte syncytium (Figures 2 and 3). However, even when we attempted to push the system, we could not evoke intercellular calcium waves (compare Figures 2 and 4). These data suggest that *in situ*, neither IP_3 nor calcium diffuses through the gap junctions that connect astrocytes *in vivo*, nor do rapid and cell-wide rises in intracellular calcium cause the release of gliotransmitters that result in intercellular waves. Finally, there have been a few studies using UV uncaging *in vivo* (*16*, *17*), and this work is, to our knowledge, the first example of two-photon uncaging in living mice. The increased depth penetration of IR light and highly localized nature of 2P excitation (compared to UV−visible, 1P excitation) make this approach particularly attractive for acute studies of signaling processes in living mice with single cell or subcellular precision.

Conclusions

We have developed a reliable synthesis of a 2P sensitive caged IP_3 analogue that may be loaded into intact astrocytes in the cortex of living mice. Using this probe, we have studied the intrinsic astrocytic calcium transients in layer 1 of the somatosensory cortex *in vivo* using 2P microscopy. In healthy mice, we found that signaling in the cell bodies is quite infrequent and is typically restricted to a single cell. Two-photon uncaging of IP_3 allowed us to mimic such activity *in vivo*. Such uncaging never evoked signaling to adjacent astrocytes. In contrast, we consistently observed intercellular calcium waves in transgenic murine models of Alzheimer's disease. Taken together, our data suggest that, in addition to the canonical IP_3 signaling mechanism that has been so well studied in astrocytes in the past 15 years, such long-range signaling events in AD mice may involve pathological release of gliotransmitters, for example, ATP.

Methods

Synthesis

(±)-1-*O*-Camphanyl-2,3−4,5-di-*O*-cyclohexylidene-6-*O*-(ortho-nitroveratryl)-*myo*-inositol (3). To a solution of

DOI: 10.1021/cn100052v | *ACS Chem. Neurosci.* (2010), *1*, 575–585

(±)-2,3−4,5-di-*O*-cyclohexylidene-6-*O*-(ortho-nitroveratryl)-*myo*-inositol (**2**) (0.20 g, 0.37 mmol) and triethylamine (0.5 mL) in methylene chloride (4 mL) was added (1*S*)-(−)-camphanic chloride (0.20 g, 0.90 mmol). The RM was stirred at RT for 18 h, diluted with methylene chloride, and washed with $NaHCO_3$ solution and saturated NaCl solution, dried with $MgSO_4$, and concentrated *in vacuo*. Flash chromatography with 20% ethyl acetate in hexane gave **3** (0.23 g) in 85% yield.

^{1}H NMR: (300 MHz, $CDCl_3$) (NB: the diastereomers appear throughout this spectrum) 7.70 and 7.69 (s, 1H); 7.40 and 7.39 (s, 1H); 5.48−5.45 (m, 1H); 5.17 (Abq, J = 55.4, 15.0 Hz, 2H); 4.70−4.65 (m, 1H); 4.50 (dd, J = 8.0, 5.1 Hz); 4.10−3.99 (m, 3H); 3.99 (s, 3H); 3.97 (s, 3H); 3.80−3.72 (m, 1H); 2.53−2.42 (m, 1H); 2.08−1.83 (m, 2H); 1.77−1.40 (m, 20H); 6 singlets for camphor methyl gropus, 1.14; 1.07; 1.05; 1.04; 0.89; 0.85.

The presence of diastereomers renders the ^{13}C NMR very complex.

HRMS: $C_{37}H_{49}NO_{13}$ requires 715.3204; 715.3238 (M^+) found.

(±)-2,3-*O*-Cyclohexylidene-6-*O*-(ortho-nitroveratryl)-*myo*-inositol (5). To a solution of **3** (0.130 g, 0.167 mmol) in 10% methanol in methylene chloride (3 mL) at 5−10 °C was added acetyl chloride (0.10 mL). The progress of the reaction was monitored carefully by TLC until almost all of **3** had disappeared. The RM was quenched with triethyl amine and concentrated *in vacuo* to give **4** that was pure enough for the next step. To a solution of crude **4** in 50% methanol in methylene chloride (5 mL) was added 1 N KOH (0.5 mL), and the RM was stirred at RT for 18 h. The RM was diluted with methylene chloride (25 mL) and with water, then saturated NaCl solution, dried with $MgSO_4$, and concentrated *in vacuo*. Flash chromatography with ethyl acetate gave **5** (0.075 g) in 100% yield.

^{1}H NMR: δ (300 MHz, $CDCl_3$) 7.69 (s, 1H), 7.34 (s, 1H), 5,23 (s, 1H), 4.44 (dd, J = 5.9, 4.1 Hz, 1H), 4.08 (dd, J = 7.4, 5.8 Hz, 1H), 4.00 (s, 3H), 4.02−3.98 (m, 1H), 3.95, (s, 3H), 3.88−3.81 (m, 1H), 3.72 (t, J = 7.8 Hz, 1H), 3.52−3.45 (m, 1H), 2.76 (d, J = 2.6 Hz, 1H), 2.66 (d, J = 2.8 Hz, 1H), 2.51 (d, J = 6.3 Hz, 1H), 1.74−1.42 (m, 10H).

The presence of diastereomers renders the ^{13}C NMR very complex.

HRMS: $C_{21}H_{29}NO_{10}$ 455.1791; 455.1778 (M^+) found.

(±)-2,3-*O*-Cyclohexylidene-6-*O*-(*ortho*-nitroveratryl)-*myo*-inositol 1,4,5-trisphosphate hexakis(2-cyanoethyl)ester (6). To a solution of **5** (0.112 g, 0.25 mmol) and *N*,*N*-diisopropyl-bis(2-cyanoethyl)-phosphoramidite (0.42 g, 1.5 mmol) in methylene chloride (6 mL) was added tetrazole (0.10 g, 1.5 mmol) in acetonitrile (4 mL) at RT. When the RM showed one spot on TLC (ca. 18 h), it was cooled to 5−10 °C, and *tert*-butyl hydrogenperoxide (0.4 mL of 30% solution in water) was added. The clear RM was allowed to warm to RT. After stirring for 3 h, the RM was diluted with methylene chloride (20 mL) and washed with water (10 mL), saturated $NaHCO_3$ (10 mL), and saturated NaCl solution (20 mL), dried with $MgSO_4$, and concentrated *in vacuo*. Flash chromatography with 5% methanol in methylene chloride gave **6** (0.142 g) in 56% yield.

^{1}H NMR: δ (300 MHz, $CDCl_3$) 7.69 (s, 1H), 7.30 (s, 1H), 5.16 (ABq, J = 42.1, 13.7 Hz, 2H), 4.91−4.86 (m, 1H), 4,83 (dd, J = 14.0, 8.4 Hz, 1H), 4.68 (dd, J = 8.7, 5.8 Hz, 1H), 4.66−4.62 (m, 1H), 4.42−4.21 (m, 14H), 4.04 (s, 3H), 3.96 (s, 3H), 2.86−2.80 (m, 8H), 2.79−2.66 (m, 4H), 1.80−1.25 (m, 10H).

^{13}C NMR: δ (70 MHz, acetone-d_6) 156.56, 150.36, 141.28, 131.93, 119.90, 119.82, 119.66, 119.48, 119.41, 114.92, 112.92, 110.34, 82.72, 80.68, 78.56, 77.32, 76.15, 73.27, 65.74, 65.65, 65.58, 65.47, 65.40, 65.34, 58.59, 58.24, 39.33, 36.98,27.29, 26.50, 26.24, 21.71, 21.66, 21.61, 21.47, 21.36.

^{31}P NMR: δ (121 MHz, $CDCl_3$) −1.75, −2.14, −2.23.

HRMS: $C_{39}H_{50}N_7O_{19}NaP_3$ requires 1036.2272; 1036.2309 (M + Na) found.

(±)-2,3-*O*-Cyclohexylidene-6-*O*-(ortho-nitroveratryl)-*myo*-inositol 1,4,5-trisphosphate hexakis(acetoxymethyl)ester (1). To a solution of **6** (0.052 g, 0.051 mmol) in acetonitrile (2 mL) was added ethyldiisopropyl amine (1 mL), and the RM was stirred at RT. After 18 h, the RM was concentrated *in vacuo* and redissolved in dry acetonitrile (3 mL) to which was added ethyldiisopropylamine (0.3 mL) and acetoxymethyl bromide (0.20 mL). The RM was stirred for 19 h at RT when HPLC analysis revealed essentially one peak. Flash chromatography with 5% methanol in methylene chloride gave **1** (0.02 g) in 35% yield.

^{1}H NMR: δ (300 MHz, $CDCl_3$) 7.71 (s, 1H), 7.47 (s, 1H), 5.74−5.61 (m, 8H), 5.47−5.41 (m, 2H), 5.40−5.24 (m 2H), 0.20 (s, 2H), 4.81 (td, J = 8.5, 3.7 Hz, 1H), 4.72 (dt, J = 8.8, 6.6, 1H), 4.64−4.54 (m, 2H), 4.31 (t, J = 6.2 Hz, 1H), 4.19 (t, J = 7,5 Hz, 1H), 4.05 (s, 3H), 3.95 (s, 3H), 2.15 (s, 3H), 2.14 (s, 3H), 2.13 (s, 3H), 2.11 (s, 3H), 2.03 (s, 3H), 2.01 (s, 3H), 1.82−1.41 (m, 10H).

^{31}P NMR: δ (121 MHz, $CDCl_3$) −3.67, −3.71, −3.96.

HRMS: $C_{39}H_{56}NO_{31}P_3Na$ requires 1150.1947; 1150.1965 (M + Na) found.

Rodent Surgery

Mice were anesthetized with an intraperitoneal injection of a 0.1 mg/kg xylazine/ketamine (each at 0.01 mg/g) mixture and supplemented with 20% of the initial dose, as needed. For some studies, 1.5 mg/g urethane was used. The level of anesthesia was checked using the paw pinch test. Once fully anesthetized, all hair on the scalp was removed using a razor-blade. A midline incision in the skin was made from the base of the skull to the base of the nose. The periosteum was cleaned from the skull with a cotton swab, and then, the animal was held in a stereotaxic apparatus. A 3 mm craniotomy above the somatosensory cortex (2 mm from the midline and −2 mm from bregma) was performed using a trephine drill bit with a microdrill (Fine Science Tools, CA, USA) such that the bone was translucent (thickness ca. 50 μm). A head plate was attached (cryanoacrylate glue), and then, the area of skull was removed. The dura mater was carefully removed to ensure minimal bleeding as any damage to the brain prevents efficient dye loading. The mouse was placed on a custom designed head plate holder for dye loading and imaging. Four types of mice were used: wild type C57BL/6, GFAP-eGFP (stock number 003257, Jackson Laboratories, Bar Harbor, ME), 3xTgAD, and background breeding control (bred from a gift of Dr. Catherine Choi, now commercially available from Jackson Laboratories, stock number 004807), and PDAPP (gift of Elan Pharmaceuticals). The AD mice are homozygous for

DOI: 10.1021/cn100052v | ACS Chem. Neurosci. (2010), 1, 575–585

AD transgenes. All animal work was conducted in accordance with the Institutional Animal Care and Use Committee guidelines.

Two-Photon Microscopy

Two-photon microscopy was performed with an Ultima *In Vivo* microscope (Prairie Technologies, Inc., WI, USA) with two mode-locked Ti:sapphire lasers through a XLUMPLFL20XW objective (Olympus; 0.95 numerical aperture). Imaging was using a Chameleon laser in the 900−950 nm wavelength range and uncaging was with a Verdi-Mira laser at 720 nm (both Coherent, Santa Clara, CA, USA). Probes (50 μg of SR-101, fluo-4, X-rhod-1, and **1**) were loaded either by topical application of solutions in DMSO/hepes ACSF (total volume ca. 50 μL) or microinjected into the brain using a Pico Spritzer II (General Valve Inc., NJ, USA) as described in refs *18*, *20*, and *21*).

Image Analysis

Fluorescent intensities were captured in each pixel on a 12-bit scale and displayed in two complementary pseudocolored modes in which cold (dark blue) and warm (red or white) colors represent an absolute change in fluorescence (i.e., 0−4096 levels) or a relative change in fluorescence (i.e., $\Delta F/F$, where F is the resting fluorescence and ΔF the signal increase). The former display shows clear cell morphology in Ca^{2+} dye-loaded cells throughout the entire field of view, but the latter depicts graphical increases in fluorescence during time lapse Ca^{2+} imaging. Thus, for Figures 2−4, both modes of display were used for the same data. Figures 2, 3, and 4b and Supporting Information movie 2 use the former and Figure 4a and Supporting Information movies 1 and 3 the latter.

Data Analysis

The fluorescence signal was quantified by measuring the mean pixel value of a manually selected somatic area for each frame of the image stack using ImageJ software. The values were exported to Excel, and the $\Delta F/F$ values were calculated. Fluorescence intensity of an astrocyte that reached higher than 20% of baseline fluorescence was considered a Ca^{2+} signal. Baseline fluorescence was defined as the mean fluorescence intensity of the first five frames (∼7 s) of the image stack for each astrocyte. Ca^{2+} oscillations were defined as a Ca^{2+} signal (>20% over baseline) that occurred within 150 frames (∼195 s) subsequent to the uncaging event. For intrinsic Ca^{2+} activity, the frequency of signaling in the field of view was calculated using the same parameters of fluorescence changes in the uncaging experiments. All data are expressed as the mean ± standard deviation (SD), except where otherwise noted. The Student's t test was used to determine the statistical significance ($p < 0.05$) of differences.

Supporting Information Available

Calcium oscillations evoked by two-photon uncaging of IP_3; calcium oscillations evoked by localized two-photon uncaging of IP_3; and intracellular calcium waves in PDAPP mouse. This material is available free of charge via the Internet at http://pubs.acs.org.

Author Information

Corresponding Author

* To whom correspondence should be addressed. E-mail: graham.ellis-davies at mssm.edu.

† These authors contributed equally to this work.

Funding Sources

This work was supported by NIH Grant GM53395 and the PA CURE Fund to G.C.R.E.-D.

References

1. Berridge, M. J., Bootman, M. D., and Lipp, P. (1998) Calcium: A life and death signal. *Nature 395*, 645–648.

2. Berridge, M. J., Bootman, M. D., and Roderick, H. L. (2003) Calcium signalling: dynamics, homeostasis and remodelling. *Nat. Rev. Mol. Cell Biol. 4*, 517–529.

3. Tsien, R. Y. (1989) Fluorescent probes of cell signaling. *Annu. Rev. Neurosci. 12*, 227–253.

4. Rudolf, R., Mongillo, M., Rizzuto, R., and Pozzan, T. (2003) Looking forward to seeing calcium. *Nat. Rev. Mol. Cell Biol. 4*, 579–586.

5. Ellis-Davies, G. C. R. (2008) Neurobiology with caged calcium. *Chem. Rev. 108*, 1603–1613.

6. Bushong, E. A., Martone, M. E., Jones, Y. Z., and Ellisman, M. H. (2002) Protoplasmic astrocytes in CA1 stratum radiatum occupy separate anatomical domains. *J. Neurosci. 22*, 183–192.

7. Haydon, P. G. (2001) Glia: listening and talking to the synapse. *Nature Rev. Neurosci. 2*, 185–193.

8. Fiacco, T. A., Agulhon, C., and McCarthy, K. D. (2009) Sorting out astrocyte physiology from pharmacology. *Annu. Rev. Pharmacol. Toxicol. 49*, 151–174.

9. Volterra, A., and Meldolesi, J. (2005) Astrocytes, from brain glue to communication elements: the revolution continues. *Nature Rev. 6*, 626–640.

10. Ellis-Davies, G. C. R. (2007) Caged compounds: photorelease technology for control of cellular chemistry and physiology. *Nature Methods 4*, 619–628.

11. Mayer, G., and Heckel, A. (2006) Biologically active molecules with a "light switch". *Angew. Chem., Int. Ed. 45*, 4900–4921.

12. Gotz, J., and Ittner, L. M. (2008) Animal models of Alzheimer's disease and frontotemporal dementia. *Nature Rev. Neurosci. 9*, 532–544.

13. Kantevari, S., Hoang, C. J., Ogrodnik, J., Egger, M., Niggli, E., and Ellis-Davies, G. C. R. (2006) Synthesis and two-photon photolysis of 6-(ortho-nitroveratryl)-caged IP3 in living cells. *ChemBioChem 7*, 174–180.

14. Dakin, K., and Li, W. H. (2007) Cell membrane permeable esters of D-myo-inositol 1,4,5-trisphosphate. *Cell Calcium 42*, 291–301.

15. Gordon, G. R., Iremonger, K. J., Kantevari, S., Ellis-Davies, G. C. R., MacVicar, B. A., and Bains, J. S. (2009)

DOI: 10.1021/cn100052v | *ACS Chem. Neurosci.* (2010), *1*, 575–585

Astrocyte-mediated distributed plasticity at hypothalamic glutamate synapses. *Neuron 64*, 391–403.

16. Godwin, D. W., Che, D., O'Malley, D. M., and Zhou, Q. (1997) Photostimulation with caged neurotransmitters using fiber optic lightguides. *J. Neurosci. Methods 73*, 91–106.

17. Takano, T., Tian, G. F., Peng, W., Lou, N., Libionka, W., Han, X., and Nedergaard, M. (2006) Astrocyte-mediated control of cerebral blood flow. *Nat. Neurosci. 9*, 260–267.

18. Hirase, H., Qian, L., Bartho, P., and Buzsaki, G. (2004) Calcium dynamics of cortical astrocytic networks in vivo. *PLoS Biol. 2*, E96.

19. Svoboda, K., and Yasuda, R. (2006) Principles of two-photon excitation microscopy and its applications to neuroscience. *Neuron 50*, 823–839.

20. Nimmerjahn, A., Kirchhoff, F., Kerr, J. N., and Helmchen, F. (2004) Sulforhodamine 101 as a specific marker of astroglia in the neocortex in vivo. *Nature Methods 1*, 31–37.

21. Stosiek, C., Garaschuk, O., Holthoff, K., and Konnerth, A. (2003) In vivo two-photon calcium imaging of neuronal networks. *Proc. Natl. Acad. Sci. U.S.A. 100*, 7319–7324.

22. Oddo, S., Caccamo, A., Shepherd, J. D., Murphy, M. P., Golde, T. E., Kayed, R., Metherate, R., Mattson, M. P., Akbari, Y., and LaFerla, F. M. (2003) Triple-transgenic model of Alzheimer's disease with plaques and tangles: intracellular Abeta and synaptic dysfunction. *Neuron 39*, 409–421.

23. Games, D., Adams, D., Alessandrini, R., Barbour, R., Berthelette, P., Blackwell, C., Carr, T., Clemens, J., Donaldson, T., and Gillespie, F.; et al. (1995) Alzheimer-type neuropathology in transgenic mice overexpressing V717F beta-amyloid precursor protein. *Nature 373*, 523–527.

24. Ding, S., Fellin, T., Zhu, Y., Lee, S. Y., Auberson, Y. P., Meaney, D. F., Coulter, D. A., Carmignoto, G., and Haydon, P. G. (2007) Enhanced astrocytic Ca2+ signals contribute to neuronal excitotoxicity after status epilepticus. *J. Neurosci. 27*, 10674–10684.

25. Tian, G. F., Azmi, H., Takano, T., Xu, Q., Peng, W., Lin, J., Oberheim, N., Lou, N., Wang, X., Zielke, H. R., Kang, J., and Nedergaard, M. (2005) An astrocytic basis of epilepsy. *Nat. Med. 11*, 973–981.

26. Kuchibhotla, K. V., Lattarulo, C. R., Hyman, B. T., and Bacskai, B. J. (2009) Synchronous hyperactivity and intercellular calcium waves in astrocytes in Alzheimer mice. *Science 323*, 1211–1215.

27. Takano, T., Tian, G. F., Peng, W., Lou, N., Lovatt, D., Hansen, A. J., Kasischke, K. A., and Nedergaard, M. (2007) Cortical spreading depression causes and coincides with tissue hypoxia. *Nat. Neurosci. 10*, 754–762.

28. Chuquet, J., Hollender, L., and Nimchinsky, E. A. (2007) High-resolution in vivo imaging of the neurovascular unit during spreading depression. *J. Neurosci. 27*, 4036–4044.

29. Green, K. N., Demuro, A., Akbari, Y., Hitt, B. D., Smith, I. F., Parker, I., and LaFerla, F. M. (2008) SERCA pump activity is physiologically regulated by presenilin and regulates amyloid beta production. *J. Cell Biol. 181*, 1107–1116.

30. Cheung, K. H., Shineman, D., Muller, M., Cardenas, C., Mei, L., Yang, J., Tomita, T., Iwatsubo, T., Lee, V. M., and Foskett, J. K. (2008) Mechanism of Ca^{2+} disruption in Alzheimer's disease by presenilin regulation of $InsP_3$ receptor channel gating. *Neuron 58*, 871–883.

31. Green, K. N., and LaFerla, F. M. (2008) Linking calcium to Abeta and Alzheimer's disease. *Neuron 59*, 190–194.

32. Arcuino, G., Lin, J. H., Takano, T., Liu, C., Jiang, L., Gao, Q., Kang, J., and Nedergaard, M. (2002) Intercellular calcium signaling mediated by point-source burst release of ATP. *Proc. Natl. Acad. Sci. U.S.A. 99*, 9840–9845.

33. Cornell-Bell, A. H., Finkbeiner, S. M., Cooper, M. S., and Smith, S. J. (1990) Glutamate induces calcium waves in cultured astrocytes: long-range glial signaling. *Science 247*, 470–473.

34. Takata, N., and Hirase, H. (2008) Cortical layer 1 and layer 2/3 astrocytes exhibit distinct calcium dynamics in vivo. *PLoS ONE 3*, e2525.

DOI: 10.1021/cn100052v | *ACS Chem. Neurosci.* (2010), *1*, 575–585